

LARGE-SCALE VECTOR MODES AND THE FIRST CMB TEMPERATURE MULTIPOLES

J. A. MORALES AND D. SÁEZ

Departamento de Astronomía y Astrofísica, Universidad de Valencia, 46100, Burjassot, Valencia, Spain;
 antonio.morales@uv.es, diego.saez@uv.es

Received 2007 October 25; accepted 2008 January 22

ABSTRACT

Recent observations have pointed out various anomalies in some multipoles (small ℓ) of the cosmic microwave background (CMB). In this paper, it is proved that some of these anomalies could be explained in the framework of a modified concordance model, in which there is an appropriate distribution of vector perturbations with very large spatial scales. Vector modes are associated with divergenceless (vortical) velocity fields. Here, the generation of these modes is not studied in detail (it can be done “a posteriori”); on the contrary, we directly look for the distributions of these vector modes which lead to both alignments of the second and third multipoles and a planar octopole. A general three-dimensional (3D) superimposition of vector perturbations does not produce any alignment, but we have found rather general 2D superimpositions leading to anomalies similar to the observed ones; in these 2D cases, the angular velocity has the same direction at any point of an extended region, and moreover, this velocity has the same distribution in all the planes orthogonal to it. Differential rotations can be seen as particular cases, in which the angular velocity only depends on the distance to a rotation axis. Our results strongly suggest that appropriate mixtures of scalar and vector modes with very large spatial scales could explain the observed CMB anomalies.

Subject headings: cosmic microwave background — cosmology: theory — large-scale structure of universe

Online material: color figures

1. INTRODUCTION

The analysis of the data obtained by the *Wilkinson Microwave Anisotropy Probe* (*WMAP*) has pointed out some anomalies in the temperature distribution of the cosmic microwave background (CMB). These anomalies have not been explained in the framework of the concordance model, which is an inflationary flat universe with cold dark matter, dark energy, and reionization. For appropriate values of the involved parameters, this model explains most of the current cosmological observations, e.g., the magnitude-redshift relation satisfied by far supernovae, the statistical properties of galaxy surveys, and the CMB anisotropies; nevertheless, some aspects of these observations remain controversial. Among them, the *WMAP* anomalies deserve attention. Some of these anomalies could be due to unexpected systematic errors associated with foreground subtraction, galactic cuts, statistical analysis, and so on; however, other anomalies could be true effects requiring new physics. Future experiments such as *Planck* should distinguish between physical effects and systematic errors. Let us now list the main anomalies: (1) the amplitude of the C_2 multipole is lower than was expected, (2) there is an asymmetry between the north and south ecliptic hemispheres, (3) the multipole C_3 is too planar, and (4) the multipoles C_2 and C_3 are too aligned. Other anomalies concerning $\ell > 3$ multipoles have also been described.

The importance of anomaly 1 was initially overestimated. The probability assigned by Spergel et al. (2003) to the C_2 value obtained from the first-year *WMAP* data was $\sim 1.5 \times 10^{-3}$. Afterward, other authors (Efstathiou 2003, 2004; Gaztañaga et al. 2003; Slosar et al. 2004) obtained greater probabilities by using different methods for data analysis. Finally, Hinshaw et al. (2007) used the data from the first three years of the *WMAP* sky survey, plus appropriate statistical and foreground subtraction techniques, to conclude that the probability of the measured C_2 multipole is ~ 0.16 . In conclusion, the observed value of C_2 is currently considered small but compatible with the concordance model. Nevertheless, a lack of correlations at the largest angular scales appears to be

statistically significant in cut-sky maps (see Spergel et al. 2003; Copi et al. 2007; Hajian 2007)

Anomaly 2 was studied in detail by Eriksen et al. (2004a, 2004b) and Hansen et al. (2004a, 2004b). The hemispherical power asymmetry is nowadays considered substantial and robust; nevertheless, more study is necessary to get definitive conclusions (Eriksen et al. 2007).

Mathematical methods to quantify the alignment of C_2 and C_3 as well as the planar character of C_3 were depicted by de Oliveira-Costa et al. (2004; vectors \mathbf{n}_2 and \mathbf{n}_3 and parameter t) and Copi et al. (2004; multipole vectors). For the sake of simplicity, we have designed a code to compute \mathbf{n}_2 , \mathbf{n}_3 , and t , whereas multipole vectors will be considered elsewhere. Vectors \mathbf{n}_2 and \mathbf{n}_3 maximize the quantity

$$\Psi = \sum_m m^2 |a_{\ell m}(\mathbf{n})|^2 \quad (1)$$

for $\ell = 2$ and 3, respectively. In this last equation, quantities $a_{\ell m}(\mathbf{n})$ are the spherical harmonic coefficients of the CMB map in a coordinate system where \mathbf{n} coincides with the z -axis. See de Oliveira-Costa et al. (2004) for the explicit definition of parameter t . Anomalies 3 and 4 have been studied in many papers (Schwarz et al. 2004; Bielewicz et al. 2004; Copi et al. 2006, 2007). The planar shape of C_3 has been confirmed by Copi et al. (2006, 2007), but this characteristic of the octopole is not very unlikely in the concordance model. More problematic is the strong alignment of C_2 and C_3 . Some authors state that the multipole alignment is actually anomalous and also that the alignment extends up to $\ell = 5$. They suggest the existence of a symmetry axis (Land & Magueijo 2005, 2007; Bernui et al. 2007; Cho 2007). Other authors (Rackić & Schwarz 2007) propose the existence of a preferred plane without rotational symmetry. This proposal suggests either a differential rotation viewed from an arbitrary point in space, which should be outside the rotation axis, or a more

complicated vortical motion with aligned angular velocities. Motions of this type—in extended regions—can be simulated with appropriate combinations of large-scale vector modes. Finally, let us mention another CMB anomaly which has been found at smaller angular scales: a non-Gaussian cold spot ($\sim 10^\circ$ size) located in the south hemisphere (Vielva et al. 2004; Cruz et al. 2005; Martínez-González et al. 2006).

An anisotropic Bianchi VII_h model has been recently considered (Jaffe et al. 2005, 2006a, 2006b; Bridges et al. 2007; Ghosh et al. 2007) with the essential aim of explaining most of the above *WMAP* anomalies; however, the authors recognize that their model does not explain the observed acoustic peaks. Other authors have studied the anisotropy produced by big voids with appropriate locations (Inoue & Silk 2006, 2007) to account for the mentioned anomalies. Motivated by the above considerations about symmetries and vortical (divergenceless) motions, we propose here another possibility which may contribute to explain the large angular scale CMB structure: the existence of vector perturbations with large enough spatial scales. Here, the main features of the first ℓ multipoles produced by these vector modes are estimated in the framework of a concordance model.

By using appropriate large scales, only their contribution to the first multipoles are significant, and consequently, there are no problems with the acoustic peaks. In the linear regime, scalar, vector, and tensor modes (Bardeen 1980) do not couple among them; hence, vector modes can be separately studied. Vector modes are vortical peculiar velocity fields which do not appear in standard inflation; nevertheless, large-scale vector modes may appear in brane-world cosmologies (Maartens 2000) and also in models with appropriate topological defects (Bunn 2002). Whatever the origin of the vector modes may be, we are interested in their possible effects on the CMB when their amplitudes are appropriately normalized. Two effects produced by the same type of large-scale vector perturbations were studied in Morales & Sáez (2007, hereafter Paper I). Some basic aspects concerning these perturbations can be found in this reference.

Our background is the so-called *concordance cosmological model*, with a reduced Hubble constant $h = 10^{-2}H_0 = 0.71$ (where H_0 is the Hubble constant in units of $\text{km s}^{-1} \text{Mpc}^{-1}$). The density parameters of vacuum energy and matter (baryonic plus dark) are $\Omega_\Lambda = 0.73$ and $\Omega_m = 0.27$, respectively. All these parameters are compatible with the analysis of the three-year *WMAP* data recently published (Spergel et al. 2007).

Throughout this paper, Greek (Latin) indices run from 0 to 3 (1 to 3). Units are defined in such a way that $c = \kappa = 1$, where c is the speed of light and $\kappa = 8\pi G/c^4$ is the Einstein constant. The unit of length is the Megaparsec. Symbols a , η , and z stand for the scale factor, the conformal time, and the redshift, respectively. Whatever quantity A may be, A_0 (A_e) stands for the value of A at the present (CMB emission) time. Quantity a_0 is assumed to be unity. This choice is always possible in a flat background.

2. CMB ANISOTROPY

The most general vector perturbation of an FRW universe is a fluctuation of the metric $g_{\alpha\beta}$, the four-velocity \mathbf{u}^α , and the traceless tensor $E_{\alpha\beta}$ describing anisotropic stresses. In the absence of scalar and tensor perturbations, the gauge can be chosen in such a way that the line element reduces to

$$ds^2 = a^2(-d\eta^2 + 2h_i dx^i d\eta + \delta_{ij} dx^i dx^j), \quad (2)$$

where the perturbations of the g_{0i} metric components have been written in the form $h_i = \{h_1, h_2, h_3\}$, $(h_1, h_2, h_3) = \mathbf{h}$. From the

matter four-velocity, $\mathbf{u}^\alpha = (u^0, \mathbf{u})$, one defines the peculiar velocity $\mathbf{v} = \mathbf{u}/u^0$. Finally, the condition $E_{ij} = 0$ is assumed throughout the paper, which means that there are no anisotropic stresses conditioning the evolution of \mathbf{v} and \mathbf{h} .

Let us now calculate the CMB temperature contrast, $\Delta T/T$, due to the above linear vector perturbations. From the equations of the null geodesics, the following formula can be easily obtained,

$$\frac{\Delta T}{T} = \mathbf{v}_{c0} \cdot \mathbf{n} - \mathbf{v}_{ce} \cdot \mathbf{n} - n^i n^j \int_{\eta_0}^{\eta_e} \frac{\partial h_j}{\partial x^i} d\eta, \quad (3)$$

where \mathbf{n} is the unit vector in the observation direction and $\mathbf{v}_c = \mathbf{v} + \mathbf{h}$. In the case of linear vector modes, the integral can be calculated along radial null geodesics of the FRW background, whose equations are $\dot{\eta} = -\dot{r}$ and $\dot{\theta} = \dot{\phi} = 0$ (in terms of the spherical coordinates r , θ , and ϕ associated with x^i). The dots stand for derivatives with respect to the affine parameter.

Functions $\mathbf{h}(\eta, \mathbf{r})$ and $\mathbf{v}(\eta, \mathbf{r})$ can be expanded in terms of an appropriate basis (the fundamental harmonic vectors; see Bardeen 1980; Hu & White 1997) to write

$$\mathbf{h}(\mathbf{r}, \eta) = - \int [B^+(\mathbf{k}, \eta)\boldsymbol{\epsilon}^+(\boldsymbol{\kappa}) + B^-(\mathbf{k}, \eta)\boldsymbol{\epsilon}^-(\boldsymbol{\kappa})] \times \exp(i\mathbf{k} \cdot \mathbf{r}) d^3k, \quad (4)$$

where \mathbf{k} is the wavenumber vector, $\boldsymbol{\kappa}$ is the unit vector \mathbf{k}/k , and functions B^+ and B^- are the coefficients of the \mathbf{h} -expansion. A representation of vectors $\boldsymbol{\epsilon}^+$ and $\boldsymbol{\epsilon}^-$ is

$$\boldsymbol{\epsilon}_1^\pm = (\pm k_1 k_3 / k - ik_2) / \sigma \sqrt{2}, \quad (5)$$

$$\boldsymbol{\epsilon}_2^\pm = (\pm k_2 k_3 / k + ik_1) / \sigma \sqrt{2}, \quad (6)$$

$$\boldsymbol{\epsilon}_3^\pm = \mp \sigma / k \sqrt{2}, \quad (7)$$

where $\sigma = (k_1^2 + k_2^2)^{1/2}$ (see Paper I). Hereafter, the following compact notation is used $B^+(\mathbf{k}, \eta)\boldsymbol{\epsilon}^+(\boldsymbol{\kappa}) + B^-(\mathbf{k}, \eta)\boldsymbol{\epsilon}^-(\boldsymbol{\kappa}) = B^\pm \boldsymbol{\epsilon}^\pm$. Vector $\mathbf{v}(\eta, \mathbf{r})$ is expanded in the same way using the coefficients $v^\pm(\mathbf{k}, \eta)$. Quantities $v_c^\pm = v^\pm - B^\pm$ are gauge invariant (Bardeen 1980). Under the condition $E_{ij} = 0$, quantities $B^\pm(\mathbf{k}, \eta)$ decrease as a^{-2} in both the radiation-dominated and the matter-dominated eras (see Paper I). Therefore, vector metric perturbations being significant at decoupling (the end of inflation) would be negligible today (at decoupling). During matter domination, the following formula holds, $B^\pm(\mathbf{k}, \eta) = 6H_0^2 \Omega_m v_{c0}^\pm(\mathbf{k}) / k^2 a^2(\eta)$. Furthermore, functions v_c^\pm are proportional to a^{-1} (constant) in the matter- (radiation-) dominated era. According to these comments, vector modes producing significant effects on the CMB should not freely evolve from the early universe. Either they are produced by exotic processes (brane-worlds, strings, and so on) close enough to recombination-decoupling or they must be maintained by some field producing an appropriate $E_{ij} \neq 0$ vector component (see Paper I). Using the above expansions and evolution laws, the relative temperature variation due to the last term of equation (3) can be rewritten as

$$\frac{\Delta T}{T} = 6H_0^2 \Omega_m \int_0^{r_e} \frac{dr}{a^2(r)} F(\mathbf{r}), \quad (8)$$

where $F(\mathbf{r}) = F_{pq}(\mathbf{r}) n^p n^q$ and

$$F_{pq}(\mathbf{r}) = -i \int \frac{k_p}{k^2} v_{c0}^\pm(\mathbf{k}) \boldsymbol{\epsilon}_q^\pm(\boldsymbol{\kappa}) \exp(i\mathbf{k} \cdot \mathbf{r}) d^3k. \quad (9)$$

This last equation can be seen as a Fourier transform for each pair (p, q) of indices. After these transforms are performed for appropriate boxes and resolutions, function $F(\mathbf{r})$ and the integral in equation (8) can be easily calculated for a set of directions defining a sky CMB map. A HEALPix (see Górski et al. 1999) pixelization covering the sky with 3072 pixels is used in our simulations.

Apart from the above CMB temperature effects, vector modes produce a rotation of the polarization direction (Skrotskii effect; Skrotskii 1957). As it was proved in Paper I, the rotation angle is

$$\delta\psi = 3H_0^2\Omega_m \int_0^{r_e} \frac{dr}{a^2(r)} [\mathbf{n} \cdot \mathbf{G}(\mathbf{r})], \quad (10)$$

where

$$\mathbf{G}(\mathbf{r}) = \int \frac{v_{c0}^+ \boldsymbol{\epsilon}^+(\boldsymbol{\kappa}) - v_{c0}^- \boldsymbol{\epsilon}^-(\boldsymbol{\kappa})}{k} \exp(i\mathbf{k} \cdot \mathbf{r}) d^3k. \quad (11)$$

For the line element from equation (2), the components of the angular velocity in momentum space are $W_i = a^3 \epsilon_{ijk} W^{jk}$. From this relation and the W_{mn} components given by Bardeen (1980) one easily gets—at first order—the following formulas,

$$W_1 = iv_c^\pm (\epsilon_2^\pm k_3 - \epsilon_3^\pm k_2), \quad (12)$$

$$W_2 = iv_c^\pm (\epsilon_3^\pm k_1 - \epsilon_1^\pm k_3), \quad (13)$$

$$W_3 = iv_c^\pm (\epsilon_1^\pm k_2 - \epsilon_2^\pm k_1); \quad (14)$$

hence, the equation $k_i W_i = 0$ is identically satisfied. The resulting components only depend on the gauge invariant quantities $v_c^\pm = v_{c0}^\pm(\mathbf{k})/a$, and consequently, the angular velocity is an appropriate vector field in order to discuss the properties of the vector modes and their superimpositions in a gauge invariant way (it is not the case of the peculiar velocity).

Various appropriate choices of $v_{c0}^\pm(\mathbf{k})$ are considered further below. In each case, the angular velocity and the resulting $\Delta T/T$ and $\delta\psi$ maps are analyzed. For the $\Delta T/T$ maps, the angle formed by vectors \mathbf{n}_2 and \mathbf{n}_3 (giving the directions of the quadrupole and octopole) and the parameter t defining the planar character of the octopole (see de Oliveira-Costa et al. 2004) are calculated.

3. CMB ANISOTROPY PRODUCED BY A SINGLE VECTOR MODE

A unique vector mode \mathbf{k}_u is first considered. In this way, some ideas—which are basic to understanding the CMB effects produced by superimpositions of these modes—are pointed out. For a unique mode, we can write

$$v_{cu}^\pm(\mathbf{k}) = v_{cu}^\pm \delta(\mathbf{k} - \mathbf{k}_u) - (v_{cu}^\pm)^* \delta(\mathbf{k} + \mathbf{k}_u), \quad (15)$$

where the complex numbers $v_{cu}^\pm = v_{cuR}^\pm + iv_{cuI}^\pm$ fix the amplitude of the chosen mode and $\delta(\mathbf{k} - \mathbf{k}_u)$ and $\delta(\mathbf{k} + \mathbf{k}_u)$ are Dirac distributions. Equation (15) implies the relation $[v_{cu}^\pm(\mathbf{k})]^* = -v_{cu}^\pm(-\mathbf{k})$, which ensures that the components of the angular velocity in position space, as well as the temperature contrast $\Delta T/T$ and the Skrotskii rotation angle $\delta\psi$, are real numbers. Moreover, for a unique mode, the coordinate axis in momentum space can be chosen in such a way that $\mathbf{k}_u = (k_{u1}, 0, 0)$ with $k_{u1} = k_u > 0$, and then, equations (5)–(7) lead to

$$\epsilon_1^\pm = 0, \quad \epsilon_2^\pm = i/\sqrt{2}, \quad \epsilon_3^\pm = \mp 1/\sqrt{2}. \quad (16)$$

For the sake of simplicity in notation, the x_1 , x_2 , and x_3 components of the angular velocity are hereafter denoted W_x , W_y , and W_z , respectively. The same notation is used for the components of any other vector in position space. From equations (12)–(16) one easily gets

$$W_x = 0, \quad (17)$$

$$W_y = k_u \sqrt{2} [(v_{cuR}^+ - v_{cuR}^-) \sin \xi + (v_{cuI}^+ - v_{cuI}^-) \cos \xi], \quad (18)$$

$$W_z = k_u \sqrt{2} [(v_{cuR}^+ + v_{cuR}^-) \cos \xi - (v_{cuI}^+ + v_{cuI}^-) \sin \xi], \quad (19)$$

where $\xi = \mathbf{k}_u \cdot \mathbf{r} = k_u r \sin \theta \cos \phi$ and variables r , θ , and ϕ are spherical coordinates in position space. Analogously, from equations (9), (15), and (16) one proves that the only nonvanishing components of $F_{pq}(\mathbf{r})$ are $F_{12} = W_z/k_u^2$ and $F_{13} = -W_y/k_u^2$. As it follows from these relations and equations (18)–(19), functions F_{12} and F_{13} depend on our choice of the complex numbers v_{cu}^\pm and v_{cu}^- . Once these numbers have been chosen, the integral of the right-hand side of equation (8) can be easily written as

$$\frac{\Delta T}{T} = \frac{6\sqrt{2}H_0^2\Omega_m n^1}{k_u} [(An^2 + Bn^3)I_c + (Cn^2 + Dn^3)I_s], \quad (20)$$

where $A = v_{cuR}^+ + v_{cuR}^-$, $B = v_{cuI}^- - v_{cuI}^+$, $C = -(v_{cuI}^+ + v_{cuI}^-)$, $D = v_{cuR}^- - v_{cuR}^+$,

$$I_s = \int_0^{r_e} a^{-2}(r) \sin \xi dr, \quad (21)$$

$$I_c = \int_0^{r_e} a^{-2}(r) \cos \xi dr, \quad (22)$$

$n^1 = \sin \theta \cos \phi$, $n^2 = \sin \theta \sin \phi$, and $n^3 = \cos \theta$. The integrals from equations (21) and (22) are to be performed along each of the 3072 directions configuring our HEALPix map from emission (r_e) to observation ($r = 0$). Afterward, the resulting map can be analyzed by using our numerical code that was specially designed to get \mathbf{n}_2 , \mathbf{n}_3 , and t .

The value $k_u = 2\pi/L_u$ with $L_u = 4 \times 10^4$ Mpc has been fixed, and then, for $A = C = 0$ and $B = D = 6.6 \times 10^{-10}$ (mode 1), vectors \mathbf{n}_2 and \mathbf{n}_3 appear to be perfectly aligned in the direction (0,1,0) and the octopole is rather planar ($t = 0.93$). The total $\Delta T/T$ map is displayed in the top panel of Figure 1. The middle and bottom panels of Figure 1 show the quadrupolar and octopolar components of this map. Figure 2 has the same structure, but it corresponds to $A = B = -C = D = 3.3 \times 10^{-10}$ (mode 2). In this last case, there is no alignment. The angle formed by the vectors $\mathbf{n}_2 = (0.037, 0.706, 0.707)$ and $\mathbf{n}_3 = (-0.037, 0.706, -0.707)$ is very close to 90° , and the parameter t takes on the value $t = 0.93$ (as in the first case). Other angles and t values appear for other choices of parameters A , B , C , and D . These results strongly suggest that random superimpositions of arbitrary vector modes should not lead to aligned \mathbf{n}_2 and \mathbf{n}_3 vectors. This fact is verified in § 4 by considering a rather general 3D superimposition.

Finally, another type of vector modes (hereafter called w -modes) deserves particular attention (see § 5 for applications). In this case, the coordinate axes in momentum space are chosen in such a way that $\mathbf{k}_u = (k_{u1}, k_{u2}, 0)$, and then, the conditions $v_{cu}^+ = v_{cu}^- = v_{cu}$ are assumed. The complex number v_{cu} can be put in the form $v_{cu} = |v_{cu}| \cos \beta + i|v_{cu}| \sin \beta$. Similarly, we can write $k_{u1} = \sigma_u \cos \alpha$ and $k_{u2} = \sigma_u \sin \alpha$. The effect of a unique w -mode is now considered.

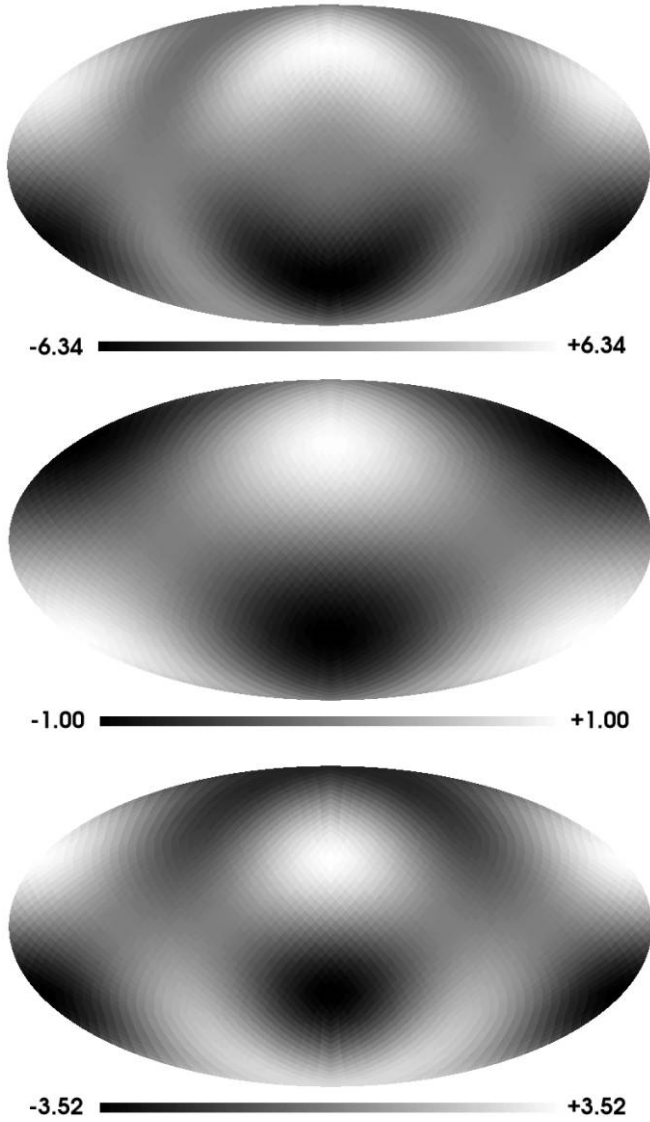


FIG. 1.—*Top*: HEALPix map of $(\Delta T/T) \times 10^5$ for vector mode 1 (see text). *Middle*: Quadrupole of this map. *Bottom*: Octopole of this map. The alignment of C_2 and C_3 is evident. The octopole looks planar. Normalization is irrelevant. [See the electronic edition of the Journal for a color version of this figure.]

By performing the same kind of calculations as for previous isolated modes, one easily gets

$$W_x = W_y = 0, \quad (23)$$

$$W_z = 2\sqrt{2}\sigma_u|v_{cu}|(\cos\beta\cos\xi - \sin\beta\sin\xi), \quad (24)$$

where $\xi = \mathbf{k}_u \cdot \mathbf{r} = \sigma_u r (n^1 \cos\alpha + n^2 \sin\alpha)$. Furthermore, the associated temperature contrast is

$$\frac{\Delta T}{T} = \frac{12\sqrt{2}H_0^2\Omega_m|v_{cu}|}{\sigma_u} (I_c \cos\beta - I_s \sin\beta) \times \left[(n^2 n^2 - n^1 n^1) \frac{\sin 2\alpha}{2} + n^1 n^2 \cos 2\alpha \right]. \quad (25)$$

Thousands of maps, M_i , corresponding to different values of α and β have been obtained and analyzed. Parameters σ_u and $|v_{cu}|$ have been fixed. Their values are $\sigma_u = \pi/(2 \times 10^4) \text{ Mpc}^{-1}$ and $|v_{cu}| = 3.3 \times 10^{-10}$. In Figure 3 we display three of these maps

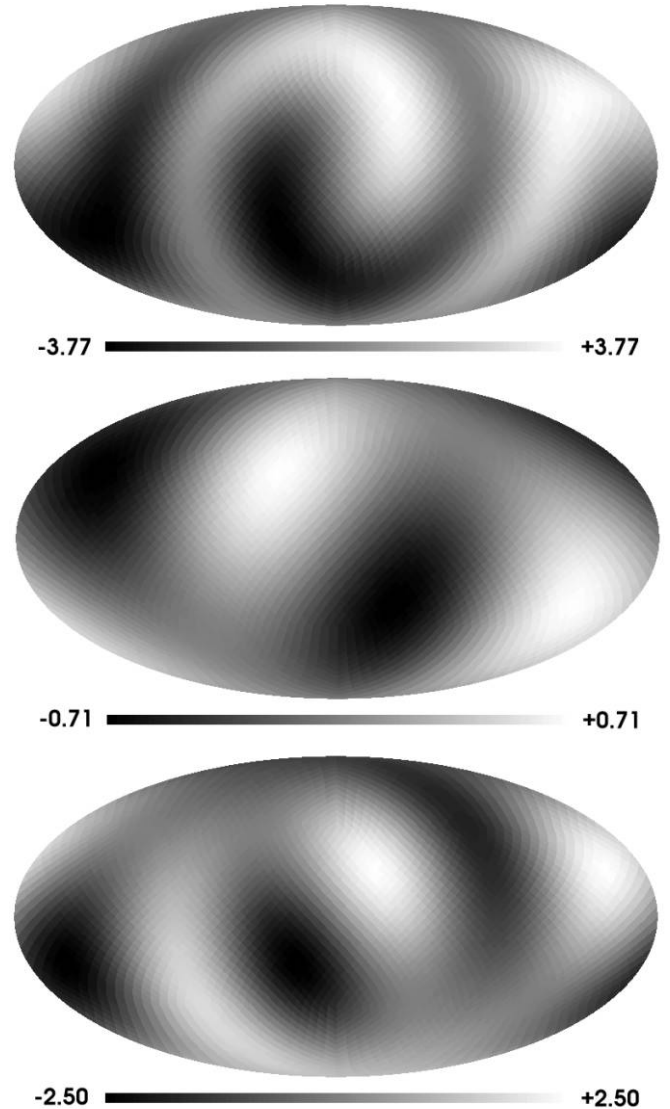


FIG. 2.—Same as Fig. 1, but for vector mode 2 (see text). There is no alignment in this case, but the octopole is visibly planar. Vectors \mathbf{n}_2 and \mathbf{n}_3 are almost orthogonal. [See the electronic edition of the Journal for a color version of this figure.]

corresponding to distinct w -modes; they are different, but the spots are always aligned along the equatorial zone, and consequently, as has been verified, vectors \mathbf{n}_2 and \mathbf{n}_3 are aligned along the direction $(0, 0, 1)$, and moreover, the octopole is very planar $t \simeq 0.94$. This type of alignment and a high t value (planar octopole) appear in all the maps. Other values of σ_u and $|v_{cu}|$ have been considered with the same result. If we superimpose many of these maps, the vectors \mathbf{n}_2 and \mathbf{n}_3 of the resulting map are not always aligned; in other words, any combination of linear modes lying in the plane (k_1, k_2) with $v_{c0}^+ = v_{c0}^- = v_{c0}$ does not lead to multipole alignments.

This fact is not surprising taking into account that, for a given map, directions \mathbf{n}_2 and \mathbf{n}_3 maximize the quantity Ψ defined in equation (1), which is *nonlinear* with respect to the $a_{\ell m}$ coefficients. Superimpositions of w -modes have been numerically analyzed in a simple way; we have taken 1521 maps M_i , and then, another 1521 maps N_j have been obtained according to the following formula, $N_j = \sum_{i=1}^j M_i$. From the analysis of the N_j maps, the following conclusions have been obtained: (1) vectors \mathbf{n}_2

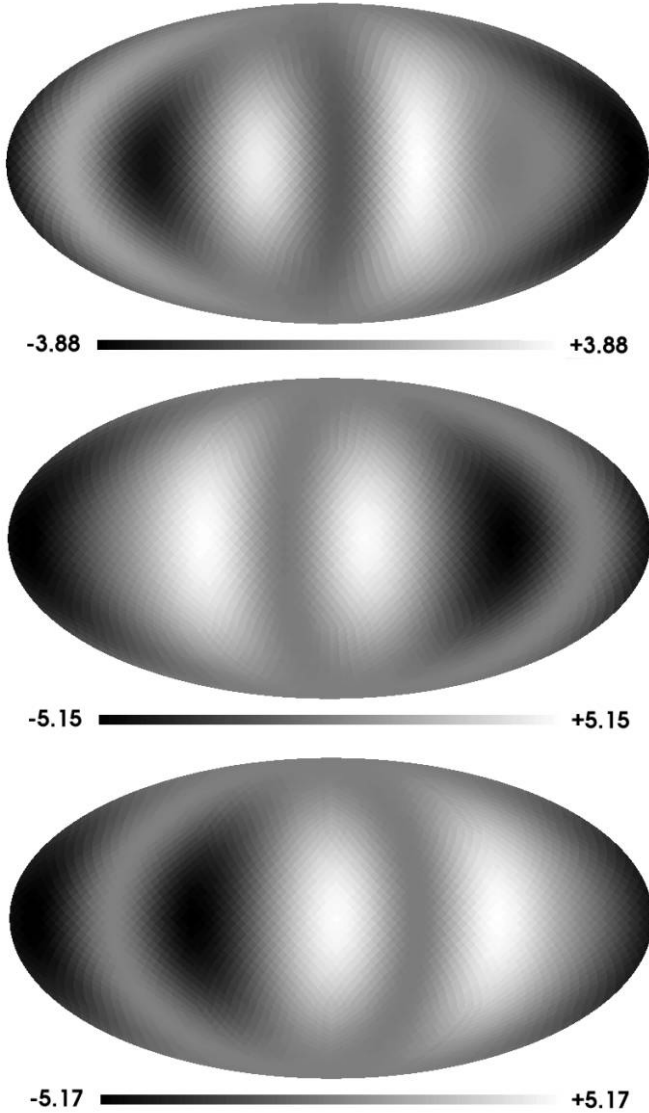


FIG. 3.—HEALPix maps of $(\Delta T/T) \times 10^5$ produced by different w -modes (see text). The equatorial alignment and the planar character of the octopole are evident in the three panels. Normalization is irrelevant. [See the electronic edition of the Journal for a color version of this figure.]

and \mathbf{n}_3 are aligned in the direction $(0,0,1)$ for 1314 of these maps, which appear to have rather planar octopoles; and (2) in the remaining 207 cases, there are no alignments and the octopole is less planar. In Figure 4, one of these cases is displayed; the spots of the bottom panel are not aligned in the equatorial zone ($t = 0.46$), and then, the direction \mathbf{n}_3 is not parallel to $(0,0,1)$. Indeed, it has been numerically verified that these directions are almost orthogonal to $(0,0,1)$ in most of the above 207 cases. A theoretical proof of this orthogonality is not easy as a result of the particular form of the *nonlinear* definition of \mathbf{n}_2 , \mathbf{n}_3 , and t . In § 5, this type of vector modes (w -modes) will be superimposed to simulate differential rotations and other symmetric divergenceless motions. Then, the fraction of the superimpositions leading to \mathbf{n}_2 and \mathbf{n}_3 alignments will be experimentally found.

4. 3D SUPERIMPOSITIONS OF VECTOR MODES

According to equation (9), functions $F_{pq}(\mathbf{r})$ can be calculated by using the 3D fast Fourier transform (FFT). In order to do

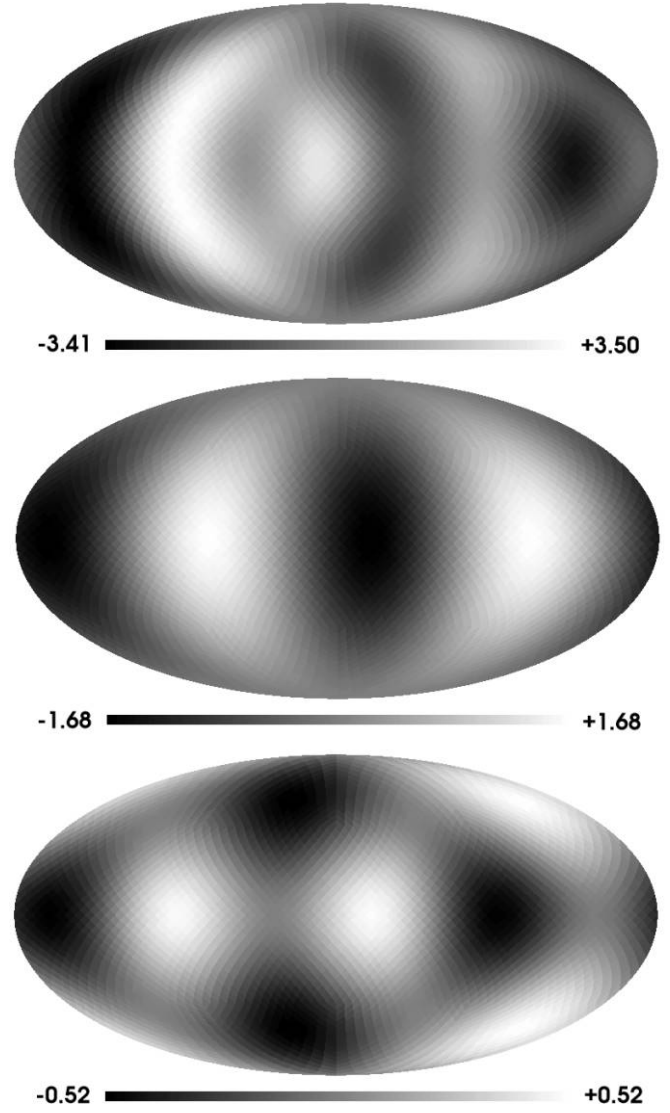


FIG. 4.—Same as Fig. 1, but for the superimposition of w -modes N_{126} (see § 3). Vector \mathbf{n}_2 has the direction $(0,0,1)$, and the octopole is not planar. Calculations indicate that vectors \mathbf{n}_2 and \mathbf{n}_3 are orthogonal; hence, direction \mathbf{n}_3 is contained in the equatorial plane. Normalization is irrelevant. [See the electronic edition of the Journal for a color version of this figure.]

that, 512^3 cells are considered inside a big box with a size of 2×10^5 Mpc. In this way, the cell size is ~ 390 Mpc, and consequently, vector modes with spatial scales between 10^4 and 5×10^4 Mpc can be well described in the simulation. We can then calculate the function $F(\mathbf{r})$ to perform the integral in equation (8); in order to do that, the observer is placed at an arbitrary point located in the central part of the simulation box, where the Fourier transform is expected to be well calculated, and then, the integration is performed for each of the 3072 directions of the pixel centers. The variations of $F(\mathbf{r})$ along the photon trajectories are smooth, and consequently, the integrations giving $\Delta T/T$ can be easily performed. Furthermore, in a central cube with 1.2×10^5 Mpc per edge (60% of the box size in our simulations), we can place 5^3 observers uniformly distributed and separated by a distance of 3×10^4 Mpc. Then, the quantity $\Delta T/T$ can be calculated for each of these observers; thus, from a given simulation the information we obtain is greater than in the case of one unique observer located, e.g., at the box center.

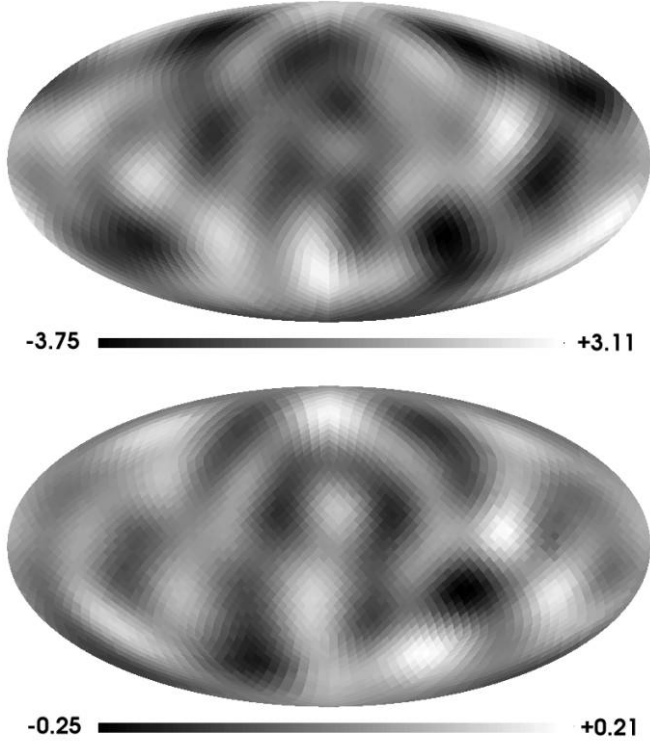


FIG. 5.—HEALPix maps of quantity $(\Delta T/T) \times 10^5$. *Top*: Part of this quantity due to the last term of eq. (3). *Bottom*: Part obtained from the term $-\mathbf{v}_{ce} \cdot \mathbf{n}$. The second part is much smaller than the first one. This is independent of the power spectrum normalization. [See the electronic edition of the *Journal* for a color version of this figure.]

In this section, it is assumed (as in Paper I) that v_{c0R}^{\pm} and v_{c0I}^{\pm} are four statistically independent Gaussian variables with vanishing mean and also that each of these numbers has the same power spectrum. The form of this common spectrum is $P(k) = Ak^{n_v}$, where n_v is the spectral index of the vector modes and A is a normalization constant. Two values of the spectral index, $n_v = 1$ and 2, have been considered. The spatial scale is varied from 10^4 to 5×10^4 Mpc in all cases (only very small k wavenumbers are considered). Four realizations of this 3D random superimposition of vector modes have been performed for each spectrum, and then, 125 observers have been located as described above in each of the simulation boxes. Thus, 500 simulations of the CMB relative temperature variations obtained from the last term of equation (3) have been obtained. Moreover, the corresponding 500 simulations of the term $-\mathbf{v}_{ce} \cdot \mathbf{n}$ have also been found. In all cases, the linearity conditions $|\mathbf{h}(\mathbf{r})| \ll 1$ and $|\mathbf{v}_c(\mathbf{r})| \ll 1$ have been verified using the relations

$$\mathbf{h}(\eta, \mathbf{r}) = -6H_0^2 \Omega_m a^{-2}(\eta) \int \frac{v_{c0}^{\pm}(\mathbf{k})}{k^2} \boldsymbol{\epsilon}^{\pm}(\boldsymbol{\kappa}) \exp(i\mathbf{k} \cdot \mathbf{r}) d^3k, \quad (26)$$

$$\mathbf{v}_c^{\pm}(\eta, \mathbf{r}) = a^{-1}(\eta) \int v_{c0}^{\pm}(\mathbf{k}) \boldsymbol{\epsilon}^{\pm}(\boldsymbol{\kappa}) \exp(i\mathbf{k} \cdot \mathbf{r}) d^3k. \quad (27)$$

The analysis of all these simulations has led to the following main results.

1. The term $-\mathbf{v}_{ce} \cdot \mathbf{n}$ is negligible against the last term of equation (3). In Figure 5, we present one simulation of each of these terms for $n_v = 1$. Numbers in the bottom panel ($-\mathbf{v}_{ce} \cdot \mathbf{n}$ term) are

much smaller than those of the top panel (last term of eq. [3]). Obviously, this comparison is independent of the spectrum normalization. We have verified that the average $\langle C_2 \rangle$ corresponding to the 500 maps of the term $-\mathbf{v}_{ce} \cdot \mathbf{n}$ is $\sim 1/600$ times smaller than the average calculated from equations (8)–(9); therefore, the term $-\mathbf{v}_{ce} \cdot \mathbf{n}$ is hereafter neglected and our study is restricted to the maps obtained from equations (8)–(9).

2. The angle α_{23} subtended by directions \mathbf{n}_2 and \mathbf{n}_3 is smaller than 10° in nine of the 500 simulations for both spectral indices, $n_v = 1$ and 2. These numbers are compatible with the 8.33 cases expected for a random distribution of direction \mathbf{n}_3 around a fixed \mathbf{n}_2 (see de Oliveira-Costa et al. 2004).

3. The parameter t appears to be greater than 0.94 in 40 and 42 simulations in the cases $n_v = 1$ and 2, respectively. These numbers are to be compared with 35, which is the corresponding number obtained by de Oliveira-Costa et al. (2004) in the case of an isotropic Gaussian random field. All these considerations are independent of the normalization of the spectra.

We can conclude that 3D random superimpositions of large-scale vector models do not explain either the observed alignment of C_2 and C_3 ($\alpha_{23} \simeq 10^\circ$) or the unusually planar octopole ($t \simeq 0.94$). However, the study of some 2D distributions of modes is worthwhile.

5. 2D SUPERIMPOSITIONS OF VECTOR MODES

Special superimpositions of vector modes are now considered. They are 2D superimpositions leading to divergenceless motions in long-sized zones, which are hereafter called *parallel vorticity regions* (PVRs). In each of these regions there is a privileged direction. Inside the region, the angular velocity (describing the local vorticity there) is parallel to the privileged direction everywhere. The x_3 -axis (hereafter z -axis) can be chosen to be parallel to the privileged direction. Finally, the PVRs are assumed to be uniform along this axis in the sense that all the orthogonal planes are equivalent. In short, inside the PVRs, the components of the angular velocity are $W_x = 0$, $W_y = 0$, and $W_z = W_z(x^1, x^2)$. This configuration appears if functions $v_{c0}^{\pm}(\mathbf{k})$ are chosen as

$$v_{c0}^+(\mathbf{k}) = v_{c0}^-(\mathbf{k}) = v_{c0}(\mathbf{k})\delta(\theta_k - \pi/2). \quad (28)$$

In this equation, angle θ_k is one of the spherical coordinates in momentum space (k and ϕ_k being the other two) and δ stands for the Dirac distribution. By substituting the distributions in equation (28) into equations (12)–(14), the following relations are obtained in position space,

$$W_x = W_y = 0, \quad (29)$$

$$W_z(x_1, x_2) = \sqrt{2} \int v_{c0}(k_1, k_2, 0) \sigma^2 e^{i(k_1 x_1 + k_2 x_2)} dk_1 dk_2. \quad (30)$$

Analogously, from equations (28) and (9), the nonvanishing components of F_{pq} appear to be

$$F_{11} = -F_{22} = -\sqrt{2} \int \frac{k_1 k_2}{\sigma^2} v_{c0}(k_1, k_2, 0) e^{i(k_1 x_1 + k_2 x_2)} dk_1 dk_2, \quad (31)$$

$$F_{12} = \sqrt{2} \int \frac{k_1^2}{\sigma^2} v_{c0}(k_1, k_2, 0) e^{i(k_1 x_1 + k_2 x_2)} dk_1 dk_2, \quad (32)$$

$$F_{21} = -\sqrt{2} \int \frac{k_2^2}{\sigma^2} v_{c0}(k_1, k_2, 0) e^{i(k_1 x_1 + k_2 x_2)} dk_1 dk_2. \quad (33)$$

Finally, vector $\mathbf{G}(\mathbf{r})$ involved in equations (10)–(11) has the following components,

$$G_x = G_y = 0, \quad (34)$$

$$G_z(x_1, x_2) = -\sqrt{2} \int v_{c0}(k_1, k_2, 0) e^{i(k_1 x_1 + k_2 x_2)} dk_1 dk_2. \quad (35)$$

As it follows from equation (28), our 2D superimpositions are combinations of the w -modes studied at the end of § 3 ($k_3 = 0$ and $v_{c0}^+ = v_{c0}^- = v_{c0}$), and consequently, vectors \mathbf{n}_2 and \mathbf{n}_3 are expected to be either parallel or orthogonal (almost in all cases). The proportions between alignments and no alignments will be numerically obtained from the analysis of simulations.

5.1. Differential Rotations

A present angular velocity of the form $W_z = W_z(\rho)$ is assumed, where $\rho = (x_1^2 + x_2^2)^{1/2}$. This velocity describes a particular PVR, which could be interpreted as a big region undergoing a differential rotation. The local vorticity only depends on the distance to the z -axis, which plays the role of the rotation axis. Then, from equation (30) one easily finds

$$v_{c0}(k_1, k_2, 0) = \frac{\sqrt{2}}{8\pi^2\sigma^2} \int W_z(\rho) e^{-i(k_1 x_1 + k_2 x_2)} dx_1 dx_2. \quad (36)$$

Function $v_{c0}(k_1, k_2, 0)$ is calculated by using the last equation, and then, this function is substituted into equations (31)–(33) to get the F_{pq} components. It is also substituted into equation (35) to obtain G_z . All these functions only depend on the coordinates x_1 and x_2 . They are easily extended inside a 3D cube (where photons move) taking into account that the planes orthogonal to the z -axis are indistinguishable. For example, in the case of the function F_{12} , its value at any point with coordinates (x^1, x^2, x^3) located inside the 3D cube would be $F_{12}(x^1, x^2, x^3) = F_{12}(x^1, x^2, 0)$. These extended functions allow us to calculate either $\Delta T/T$ (from eq. [8]) or the polarization rotation angle $\delta\psi$ (from eq. [10]). These calculations can be performed for any observer located well inside the cube, in other words, for any observer whose last scattering surface is fully localized inside the cube.

It is worthwhile to notice that, in the case of the rigid rotation of a big region, the angular velocity W_z vanishes in a certain gauge, in which the observer rotates with the region. In this gauge, equation (36) gives $v_c(k_1, k_2, 0) = 0$, and taking into account that this quantity is gauge invariant, it vanishes in any gauge; therefore, according to equations (31)–(35) plus equations (8) and (10), quantities $\Delta T/T$ and $\delta\psi$ vanish. In short, there is no CMB anisotropy or Skrotskii rotations associated with rigid rotations (the same is valid for rotations of the spatial coordinates in the absence of vector modes). These effects only appear in the case of differential rotations, which cannot be globally avoided by any rotation of the reference frame.

Two functions $W_z = W_z(\rho)$ have been used; the first one is

$$W_z^N(\rho) = \begin{cases} N_1 \left[e^{-(\rho^2/2m^2)} - e^{-2} \right], & \rho \leq 2m, \\ 0, & \rho > 2m, \end{cases} \quad (37)$$

where N_1 is a normalization constant. The length m defines the spatial size of the PVR. The values $m = 5 \times 10^3$ Mpc (case NI) and $m = 3 \times 10^3$ Mpc (case NII) have been tried. Evidently, the spatial scales involved in this differential rotation are very large. The second function is

$$W_z^C(\rho) = \begin{cases} N_2 \cos(\pi\rho/2\rho_{\max}), & \rho \leq \rho_{\max}, \\ 0, & \rho > \rho_{\max}; \end{cases} \quad (38)$$

quantities N_2 and ρ_{\max} are the normalization constant and the parameter defining the spatial profile of the angular velocity, respectively. Two values of ρ_{\max} have been studied, $\rho_{\max} = 6.8 \times 10^3$ Mpc (case CI) and $\rho_{\max} = 4 \times 10^3$ Mpc (case CII).

Once an angular velocity profile $W_z = W_z(\rho)$ has been assumed (cases NI, NII, CI, and CII), only two elements remain free: (1) the normalization constant and (2) the location of the observer in the simulation square. The square is that appropriate for the Fourier transforms in equations (31)–(35). For the above profiles, a square size of 5×10^4 Mpc is used, and then, 81 observers are uniformly located in a central square of 2×10^4 Mpc size. The separation between neighboring observers is 2.5×10^3 Mpc; therefore, once parameter m (ρ_{\max}) is fixed in the profile W_z^N (W_z^C), 81 simulations of $\Delta T/T$ and $\delta\psi$ can be obtained as has been described in the first paragraph of § 5.1. Each map corresponds to a localization of the observer characterized by its distance to the rotation axis ($x_1 = x_2 = 0$ line). The analysis of the resulting HEALPix maps has led to the following main conclusions: (1) the C_2 – C_3 alignment is perfect for any of the above W_z profiles and observers ($\alpha_{23} = 0$); and (2) the inequality $t > 0.94$ also is satisfied in all cases. These results are encouraging. The proposed differential rotations plus appropriate large-scale scalar modes could easily lead to the observed angle $\alpha_{23} \simeq 10^\circ$ and also to the parameter $t \simeq 0.94$. Of course, the large-scale vector modes under consideration should dominate against the scalar ones. Thus, the alignment produced by the differential rotation (vector modes) would not be hidden by the effects of standard scalar modes. The amplitude of the scalar perturbations contributing to small- ℓ multipoles (very large scales) should be smaller than those corresponding to the standard flat spectrum (compatible with the remaining observed C_ℓ quantities). Either a certain cutoff or a damping of the scalar fluctuations would be necessary on very large scales. Details about the possible cutoff scale or the gradual damping are out of the scope of this paper; however, the general considerations of this paragraph are important to normalize the W_z profiles.

A few considerations about recent CMB observations are necessary before describing our normalization method. According to Hinshaw et al. (2007; *WMAP* three-year data analysis), the CMB quadrupole is $C_2^{WMAP} \simeq 2.96 \times 10^{-11}$, whereas the octopole is $C_3^{WMAP} \simeq 7.38 \times 10^{-11}$; hence, if it is assumed that the contribution of scalar and vector modes to these multipoles are to be added (statistical independence of the scalar modes and the differential rotation) and, moreover, it is taken into account that the contribution of the vector modes must dominate (see previous paragraph), then such a vector contribution should roughly satisfy the following conditions: (1) C_2 must be a little smaller than 2.96×10^{-11} and (2) $2C_2 < C_3 < 3C_2$. Hence, the following method is used to normalize in each of the cases NI, NII, CI, and CII. In the first step, the C_2 and C_3 multipoles of the 81 maps are calculated for an arbitrary normalization, and then, the maps (observers) compatible with condition 2—which is independent of normalization—are found. The total number, N_b , of these maps is given—for each case—in Table 1. Some of these maps correspond to observers located at the same distance from the rotation axis, and consequently, their normalizations are identical except for small numerical errors. This fact has been verified. The total number of distinct distances (observers), N_d , and the distances themselves, $d_{or}(i)$ with $i \in [1, N_d]$, are also given in Table 1. In a second step, the normalization constant is chosen to have $C_2 = 2.5 \times 10^{-11}$ for each of the above N_d observers, and then, the resulting octopoles, $C_3(i)$, are calculated and shown in Table 1 for $i \in [1, N_d]$. A number N_d of different normalizations is thus obtained. Each of these normalizations is separately considered. The $\Delta T/T$ and $\delta\psi$ maps corresponding to one of the two observers of case

TABLE 1
2D SIMULATIONS BASED ON W_z PROFILES

Case	N_b^a	N_d^b	$C_3(1) \times 10^{11}$	$C_3(2) \times 10^{11}$	$d_{or}(1) \times 10^{-3}$ (Mpc)	$d_{or}(2) \times 10^{-3}$ (Mpc)	$A_{wz}(1) \times 10^9$	$A_{wz}(2) \times 10^9$
NI.....	12	2	7.23	5.94	7.9	9.0	0.99	0.95
NII.....	8	1	6.58	...	7.9	...	2.51	...
CI.....	12	2	7.04	5.33	7.9	9.0	1.51	1.41
CII.....	8	1	5.77	...	7.9	...	3.94	...

NOTES.—First column lists the four W_z profiles defined in the text. In each case, 81 observers are uniformly distributed in the central part of the simulation box. We also have that $C_3(1)$ is the octopole (after normalization by the condition $C_2 = 2.5 \times 10^{-11}$) of one of the N_d observers, whereas $C_3(2)$ corresponds to the second of these observers (if it exists). The same is the case for d_{or} and for the dimensionless ratio $W_z(\rho = 0)/H_0$.

^a The number of observers whose CMB multipoles satisfy the relation $2C_2 < C_3 < 3C_2$ is N_b .

^b Among the N_b observers, there are N_d ones which are actually different (they are located at distinct distances, d_{or} , from the rotation axis).

NI ($i = 1$ in Table 1) are displayed in Figure 6. The top panel shows a $\Delta T/T$ map which seems to be clearly compatible with a planar octopole (estimated value of $t \simeq 0.9979$) and a perfect alignment ($\alpha_{23} = 0$, with possible small errors due to the limited angular resolution of the HEALPix maps). The bottom panel displays the corresponding $\delta\psi$ map. Angles close to 0.1° are reached in some directions; the angles are similar to (a little smaller than) those obtained in Paper I, which were estimated by using a rather arbitrary normalization.

After the above normalization method has been applied, any of the N_d normalizations correspond to an observer (characterized by its distance to the rotation center) whose C_2 and C_3 multipoles satisfy the following conditions: (1) they are appropriate to explain the values observed by the *WMAP* satellite with the help of a certain contribution due to scalar modes (to be estimated); (2) these multipoles are fully aligned; and (3) the octopole is very planar

($t > 0.94$). The distances from the observers to the rotation axis are different from zero (see Table 1), and consequently, these observers are not placed on the rotation axis but in another position, which is as probable as any other position in the space.

Normalizations lead to the values of the constants N_1 and N_2 involved in equations (37)–(38), from which the dimensionless amplitude of the angular velocity profile $A_{wz} = W_z(\rho = 0)/H_0$ can be found in each case. The resulting A_{wz} values are given in Table 1 for the normalizations included in it. They are a few times greater than the value 4.3×10^{-10} reported by Jaffe et al. (2005) in the framework of a fully different model.

5.2. Statistical Parallel Vorticity Fields

In this section, a PVR is simulated by using statistical methods. The components v_{c0R} and v_{c0I} of the complex numbers $v_{c0}(k_1, k_2, 0)$ are generated as two statistically independent Gaussian variables with the same power spectrum and zero mean. The form of the spectrum is the same as in the 3D simulations; namely, $P(\sigma) = A\sigma^{n_v}$, and the chosen spectral indices and spatial scales are also the same as in the 3D statistical realizations.

Ten realizations of these 2D random superimposition of vector modes have been performed for each spectrum ($n_v = 1$ and 2), and then, 81 observers were uniformly located in the simulation square using the same method as in the 2D simulations with W_z profiles; however, the sizes of the simulation square and the central square are 2×10^5 and 1.28×10^5 Mpc, respectively, and the distance between observers is 1.6×10^3 Mpc. Thus, 810 simulations of the CMB relative temperature variations produced by PVRs have been obtained. The corresponding $\delta\psi$ maps have also been found. All these maps have been analyzed. Results from this analysis are now described; we begin with various conclusions which are independent of the spectrum normalizations: (1) the angle α_{23} is zero in 48.64% (48.4%) of the 810 simulations for $n_v = 1$ ($n_v = 2$); (2) the parameter t appears to be greater than 0.94 in 18.64% (19.88%) of the simulations for $n_v = 1$ ($n_v = 2$); and (3) the conditions $t > 0.94$ and $\alpha_{23} = 0$ are simultaneously satisfied in $\sim 11\%$ ($\sim 12\%$) of the simulations for $n_v = 1$ ($n_v = 2$). These last percentages can be found from Table 2, where the number of cases, n_{at} , satisfying the two relations $t > 0.94$ and $\alpha_{23} = 0$ is given for each of the 10 2D realizations. We have counted these cases, because as has been discussed in § 3, conditions $t > 0.94$ and $\alpha_{23} = 0$ do not seem to be independent and, consequently, the probability of the realizations satisfying the two relations is not a priori the product of the individual probabilities.

The spectra are normalized as follows. First, all the simulations satisfying the conditions $t > 0.94$ and $\alpha_{23} = 0$ are normalized by the condition $C_2 = 2.5 \times 10^{-11}$, and then, those of them satisfying the inequalities $2C_2 < C_3 < 3C_2$ are identified and counted.

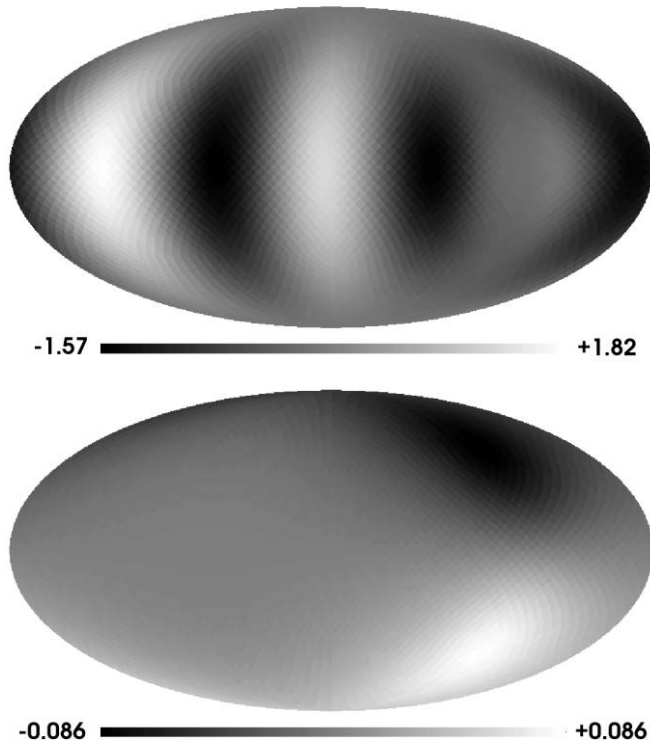


FIG. 6.—Top: HEALPix map of $(\Delta T/T) \times 10^5$ for case NI and observer $i = 1$ (see Table 1). A strong C_2 - C_3 alignment and a high t value are evident. Bottom: Corresponding $\delta\psi$ map, where the angles are given in degrees. [See the electronic edition of the *Journal* for a color version of this figure.]

TABLE 2
STATISTICAL 2D SIMULATIONS

Case ($n_v = 1$)	n_{at}^a	n_{obs}^b	Case ($n_v = 2$)	n_{at}	n_{obs}
1.....	7	1	1.....	11	3
2.....	9	0	2.....	10	1
3.....	6	2	3.....	12	2
4.....	9	1	4.....	12	2
5.....	9	0	5.....	11	2
6.....	7	3	6.....	10	1
7.....	9	0	7.....	12	2
8.....	4	0	8.....	12	1
9.....	11	1	9.....	12	2
10.....	17	0	10.....	12	0

NOTE.—Ten 2D statistical simulations corresponding to the spectral indices $n_v = 1$ and 2 are numbered in the first and fourth columns, respectively.

^a Number of observers which measure $\alpha_{23} = 0$ and $t > 0.94$ (among 81 of them placed inside the simulation box).

^b Number of cases (among 81) in which measurements would be compatible with conditions $\alpha_{23} = 0$, $t > 0.94$, and $2C_2 < C_3 < 3C_2$.

Their total number, n_{obs} , is given in Table 2 for each of our 10 2D realizations. It is worthwhile to notice that each of the normalized simulations corresponds to one of the 10 2D statistical realizations and also to an observer located at a certain position in the simulation cube. Since there is no rotation axis, coordinates x^1 and x^2 are both necessary to fix the observer position in the plane orthogonal to the vorticity direction of the PVR.

For $n_v = 1$ (2), the number n_{obs} appears to be zero in five (one) of our 10 2D statistical superimpositions of vector modes. In these five (one) cases, conditions $t > 0.94$ and $\alpha_{23} = 0$ are satisfied

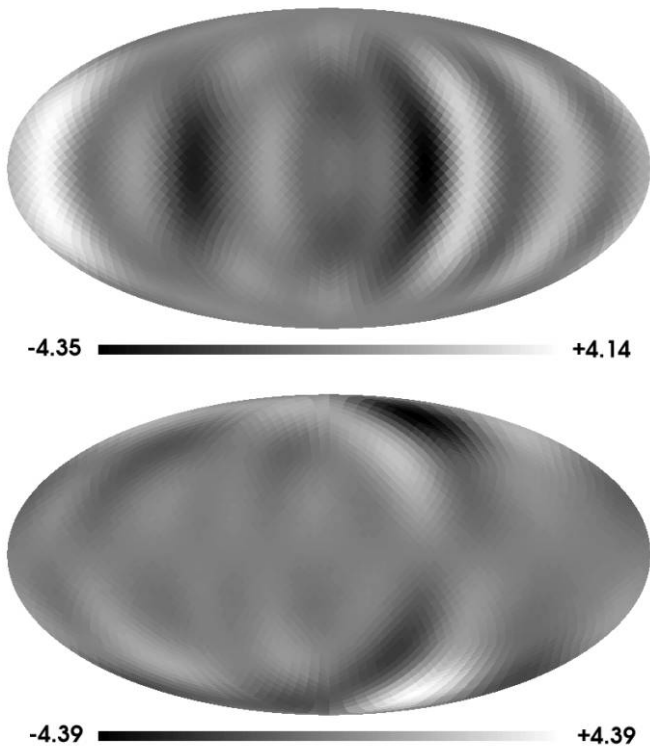


FIG. 7.—*Top*: Same as Fig. 6, but for one of the two observers measuring multipoles C_2 and C_3 compatible with current observations in realization number 9 of the case $n_v = 2$ (see Table 2 and text). *Bottom*: Corresponding Skrotskii angles, $\delta\psi$, given in units of 10^{-3} deg. [See the electronic edition of the Journal for a color version of this figure.]

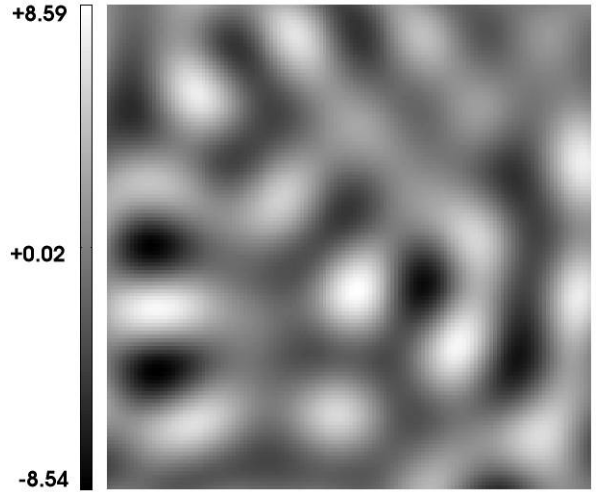


FIG. 8.—Map of the dimensionless quantity $(W_z/H)_0 \times 10^9$ in the plane orthogonal to the angular velocity. The size of the represented square is 50 Mpc. [See the electronic edition of the Journal for a color version of this figure.]

(see Table 2), but there are no observers measuring a quadrupole $C_2 = 2.5 \times 10^{-11}$ and an octopole satisfying the relations $2C_2 < C_3 < 3C_2$. It is then easy to calculate the probability of having at least one observer whose measurements satisfy the four conditions $t > 0.94$, $\alpha_{23} = 0$, $C_2 = 2.5 \times 10^{-11}$, and $2C_2 < C_3 < 3C_2$, namely, whose measurements may be compatible with current observations after introducing appropriate subdominant scalar modes. This probability is close to $\sim 5.5\%$ ($\sim 10.8\%$) for $n_v = 1$ (2). With these probabilities we cannot say that we live in a very special zone of the PVR, but in a reasonably probable one, which is equally probable to any other positions inside the PVR.

For $n_v = 2$ and 2D realization number 9 of Table 2, there are two observers ($n_{obs} = 2$) whose measurements are compatible with the four above conditions. One of these observers, located at $\sim 5 \times 10^4$ Mpc from the cube center, would measure $t \simeq 0.9631$, $\alpha_{23} = 0$, $C_2 = 2.5 \times 10^{-11}$, and $C_3 = 6.45 \times 10^{-11}$. The $\Delta T/T$ and $\delta\psi$ maps corresponding to this observer are shown in Figure 7. The top panel displays the $\Delta T/T$ map, which looks like those compatible with a planar octopole and a perfect alignment. The corresponding $\delta\psi$ map is exhibited in the bottom panel. The largest angles—close to $\sim 4.4 \times 10^{-3}$ deg—are much smaller (by a factor $\sim 1/50$) than those based on the normalization of Paper I. Of course, these angles are too small to produce any currently significant B -polarization of the CMB.

Finally, Figure 8 shows a dimensionless quantity proportional to the present angular velocity W_z . The represented zone is located inside the simulation square and centered in it. The normalization is the same as in Figure 7 (same 2D simulation and observer). White and black spots correspond to regions which are rotating in opposite senses. A boundary with $W_z = 0$ separates them. The mean value of $(W_z/H)_0$ is negligible by construction, and the typical deviation is $\langle |W_z|^2 \rangle^{1/2}/H_0 = 3 \times 10^{-9}$. Many realizations (e.g., Fig. 8) have been considered to conclude that the typical value of $(W_z/H)_0$ is always a few times 10^{-9} .

6. DISCUSSION AND CONCLUSIONS

Appropriate combinations of large-scale vector perturbations have been introduced in the concordance model, and then, their effects on the CMB anisotropy have been studied in detail. Our main conclusions can be summarized as follows: 3D superimpositions

of vector modes do not explain the CMB anomalies; however, some 2D superimpositions of these modes lead to good results. Two types of 2D simulations have been performed: one of them represents differential rotations of big regions and the other one leads to extended statistical PVRs. In these two cases there is a preferred direction of symmetry. It is the direction of the angular velocity, which is the same for any point of the perturbed region. In the first case, there is a symmetry around the rotation axis in the plane orthogonal to the preferred direction; however, statistical PVRs do not introduce such a rotational symmetry.

Suitable differential rotations can explain the planar character of the octopole, its alignment with the quadrupole, and the main part of the C_2 and C_3 values observed with *WMAP*. These facts are proved, in § 5.1, for two different W_z profiles. Polarization rotation angles $\delta\psi$ close to 0.1° are produced by these profiles. Other possible profiles could produce slightly greater angles. A subdominant contribution of large-scale scalar modes could then account for a small part of the observed quadrupole and octopole, which would be complementary to the part due to vector modes. These scalar modes could also be responsible for the observed angle $\alpha_{23} \simeq 10^\circ$, which vanishes for pure differential rotations. The required scalar modes would destroy the rotational symmetry in the plane orthogonal to the axis of the differential rotation. Skrotskii rotations close to 0.1° would produce a B -polarization of the CMB, which could be marginally observable by future satellites (see Paper I).

For statistical PVRs, there is an appreciable probability of accounting for all the anomalies explained by differential rotations. This probability depends on the form of the assumed power spectrum and also on the interval of k values considered in the computations. The dependence on the spectral index has been pointed out by considering two distinct values $n_v = 1$ and 2 (see § 5.2). The mentioned probability is greater in the case $n_v = 2$ ($\sim 11\%$). Of course, a certain level of scalar modes is necessary (as in the case of differential rotations) in order to explain the observed angle $\alpha_{23} \simeq 10^\circ$. Statistical PVRs lead to $\delta\psi$ angles which are too small to produce significant levels of B -polarization. Other intervals of spatial scales and other power spectra could lead to higher probabilities for the explanation of anomalies and, perhaps, to greater Skrotskii rotations. In a certain k interval, the spectrum of vector modes could have any form (a power law is not required either by any theoretical prediction or by observational evidence). In a finite interval, e.g., between 10^4 and 5×10^4 Mpc, the spectral index of a power spectrum is arbitrary; nevertheless, only some spectral indices are admissible, as k tends to zero, to avoid divergences in some integrals (e.g., that of eq. [31]).

In Rackić & Schwarz (2007) it is stated that, at high confidence, there is not any rotational symmetry of the CMB in the plane orthogonal to the symmetry axis. This fact is compatible with differential rotations for two reasons: (1) the mentioned rotational symmetry would be only observed from points placed on the rotation axis, whereas we are not located on this line with very high probability; and (2) there may be either large-scale subdominant scalar perturbations or deviations with respect to a perfect differential rotation, and obviously, these perturbations and deviations could contribute to hide any rotational symmetry and also to explain the deviation from zero observed in the angle α_{23} .

The asymmetry of the north and south ecliptic hemispheres is also compatible with our 2D superimpositions of vector modes. We predict two equivalent hemispheres; nevertheless, they are not separated by the ecliptic plane, but by the plane orthogonal to the angular velocity. Furthermore, in some slightly different sce-

narios, the equivalence of these two hemispheres could disappear. It occurs, e.g., if the last scattering surface of the observer is partially outside the PVR, which is particularly probable for PVRs which are not too extended in some direction.

Solar system alignments would be casual, as it seems natural in any cosmological explanation of the observed anomalies (see Cho 2007). All the theories of this type (including our proposal) would be ruled out by solutions of the CMB anomaly problem based on both the ordinary spectrum of scalar perturbations and a noncosmological component accounting for the observed statistical correlations with the local geometry of the solar system; however, current observations and data analysis have not unveiled any component of this type accounting for the CMB anomalies.

We have assumed very large spatial scales to alter only a few low- ℓ multipoles; nevertheless, only vector modes have been considered. Why have large-scale scalar modes not been tried? The main reasons are now pointed out. For the chosen spatial scales, combinations of modes should lead to very large almost homogeneous regions. It occurs whatever the nature of the perturbations may be. In the case of vector modes, the angular velocity will be almost homogeneous in these regions, and consequently, it will have almost the same direction everywhere. These absolutely natural regions, which could have sizes comparable to that of the sphere bounded by the large scattering surface (for large enough spatial scales), are the PVRs we need to explain anomalies. In the case of scalar perturbations, the density contrast should be almost constant in these large regions, and consequently, a cylindrical scalar inhomogeneity would be actually unlikely. Moreover, a flattened inhomogeneity does not seem likely as a result of the small scales required by the short thickness of the structure, which would be small enough to affect multipoles with too large ℓ values. Hence, the symmetry axis and preferred planes seem to be rather improbable in the case of large-scale scalar modes. Although these arguments are qualitative, they strongly suggest the use of vector modes.

Let us finish this paper with a list of a few open problems which should be addressed in the near future: (1) the origin and evolution laws of the vector modes (e.g., brane-worlds, strings) deserve particular attention. Only a consistent theory on these subjects could give answers to important questions such as: in what cosmological period (or periods) are the vector modes generated? How do they actually decay? How probable are the PVRs? Are scalar and vector modes statistically independent? (2) Multipole components for $\ell > 3$ must also be analyzed and compared with those extracted from *WMAP* data. Multipole vectors (Copi et al. 2004) should be used in this extended study. (3) The proportions between large-scale scalar and vector modes must be considered in more detail; and (4) deviations from the perfect parallelism assumed in our 2D superimpositions of vector modes could lead to interesting results (hemisphere asymmetry, α_{23} observed value, and so on).

Large-scale rotations are currently enigmatic (even for us), but the origin of the familiar cosmic expansion has remained unknown for a century. In both cases, rotation and expansion, rejection (acceptance) would be only justified by the disagreement (agreement) between predictions and observations (without prejudices). Although we do not have a closed theory on the subject of this paper, results related to the CMB anomalies are actually encouraging, and consequently, more study is worthwhile.

This work has been supported by the Spanish Ministerio de Educación y Ciencia, MEC-FEDER project FIS 2006-06062.

REFERENCES

- Bardeen, J. M. 1980, *Phys. Rev. D*, 22, 1882
- Bermui, A., Mota, B., Rebouças, M. J., & Tavakol, R. 2007, *A&A*, 464, 479
- Bielewicz, P., Górski, K. M., & Banday, A. J. 2004, *MNRAS*, 355, 1283
- Bridges, M., McEwen, J. D., Lasenby, A. N., & Hobson, M. P. 2007, *MNRAS*, 377, 1473
- Bunn, E. F. 2002, *Phys. Rev. D*, 65, 043003
- Cho, A. 2007, *Science*, 317, 1848
- Copi, C. J., Huterer, D., Schwarz, D. J., & Starkman, G. D. 2006, *MNRAS*, 367, 79
- . 2007, *Phys. Rev. D*, 75, 023507
- Copi, C. J., Huterer, D., & Starkman, G. D. 2004, *Phys. Rev. D*, 70, 043515
- Cruz, M., Martínez-González, E., Vielva, P., & Cayón, L. 2005, *MNRAS*, 356, 29
- de Oliveira-Costa, A., Tegmark, M., Zaldarriaga, M., & Hamilton, A. 2004, *Phys. Rev. D*, 69, 063516
- Efstathiou, G. 2003, *MNRAS*, 346, L26
- . 2004, *MNRAS*, 348, 885
- Eriksen, H. K., Banday, A. J., Górski, K. M., Hansen, F. K., & Lilje, P. B. 2007, *ApJ*, 660, L81
- Eriksen, H. K., Banday, A. J., Górski, K. M., & Lilje, P. B. 2004a, *ApJ*, 612, 633
- Eriksen, H. K., Hansen, F. K., Banday, A. J., Górski, K. M., & Lilje, P. B. 2004b, *ApJ*, 605, 14
- Gaztañaga, E., Wagg, J., Multamäki, T., Montaña, A., & Hughes, D. H. 2003, *MNRAS*, 346, 47
- Ghosh, T., Hajian, A., & Souradeep, T. 2007, *Phys. Rev. D*, 75, 083007
- Górski, K. M., Hivon, E., & Wandelt, B. D. 1999, in *Proc. MPA-ESO Cosmology Conf.*, ed. A. J. Banday, R. K. Sheth, & L. N. da Costa (Garching: European Southern Observatory), 37 (astro-ph/9812350)
- Hajian, A. 2007, preprint (astro-ph/0702723)
- Hansen, F. K., Balbi, A., Banday, A. J., & Górski, K. M. 2004a, *MNRAS*, 354, 641
- Hansen, F. K., Banday, A. J., & Górski, K. M. 2004b, *MNRAS*, 354, 641
- Hinshaw, G., et al. 2007, *ApJS*, 170, 288
- Hu, W., & White, M. 1997, *Phys. Rev. D*, 56, 596
- Inoue, K. T., & Silk, J. 2006, *ApJ*, 648, 23
- . 2007, *ApJ*, 664, 650
- Jaffe, T. R., Banday, A. J., Eriksen, H. K., Górski, K. M., & Hansen, F. K. 2005, *ApJ*, 629, L1
- . 2006a, *ApJ*, 643, 616
- . 2006b, *A&A*, 460, 393
- Land, K., & Magueijo, J. 2005, *Phys. Rev. Lett.*, 95, 071301
- . 2007, *MNRAS*, 378, 153
- Maartens, R. 2000, *Phys. Rev. D*, 62, 084023
- Martínez-González, E., Cruz, M., Cayón, L., & Vielva, P. 2006, *NewA Rev.*, 50, 875
- Morales, J. A., & Sáez, D. 2007, *Phys. Rev. D*, 75, 043011 (Paper I)
- Rackić, A., & Schwarz, D. J. 2007, *Phys. Rev. D*, 75, 103002
- Schwarz, D. J., Starkman, G. D., Huterer, D., & Copi, C. J. 2004, *Phys. Rev. Lett.*, 93, 221301
- Skrotskii, G. V. 1957, *Soviet Phys. Dokl.*, 2, 226
- Slosar, A., Seljak, U., & Makarov, A. 2004, *Phys. Rev. D*, 69, 123003
- Spergel, D. N., et al. 2003, *ApJS*, 148, 175
- . 2007, *ApJS*, 170, 377
- Vielva, P., Martínez-González, E., Barreiro, R. B., Sanz, J. L., & Cayón, L. 2004, *ApJ*, 609, 22